MAVEN Survey of Magnetic Flux Rope Properties in the Martian Ionosphere: Comparison with 3 Types of Formation Mechanisms

Charles Bowers[1], James A. Slavin[1], Gina A. DiBraccio[2], Gangkai Poh[3], Takuya Hara[4], Shaosui Xu[5], and David Andrew Brain[6]

[1]University of Michigan-Ann Arbor
[2]NASA GSFC
[3]Catholic University of America
[4]University of California, Berkeley
[5]Space Sciences Lab, UC Berkeley
[6]University of Colorado Boulder

November 24, 2022

Abstract

Flux ropes are a magnetic field phenomenon characterized by a filament of twisted magnetic field with an axial core and outer helical wraps. They form in the Martian ionosphere via three distinct mechanisms: boundary wave instabilities (BWI), external reconnection (ER) between the interplanetary magnetic field and the crustal anomalies, and internal reconnection (IR) of the crustal anomalies themselves. We have identified 121 magnetic flux ropes from 1900 orbits using plasma and magnetic field measurements measured by the Mars Atmosphere and Volatile EvolutioN (MAVEN) spacecraft, and separate flux ropes into categories based on formation mechanism by analyzing electron signatures. We find evidence for flux ropes formed via BWI, ER, and IR mechanisms which comprise 9%, 34%, and 57% of our dataset, respectively. Flux ropes formed via different mechanisms exhibit differences in location and force-free radius, indicating the formation mechanism of a flux rope impacts their influence on the Martian plasma environment.

MAVEN Survey of Magnetic Flux Rope Properties in the Martian Ionosphere: Comparison with 3 Types of Formation Mechanisms

C. F. Bowers[1], J. A. Slavin[1], G. A. DiBraccio[2], G. Poh[2,3], T. Hara[4], S. Xu[4], D.A. Brain[5]

[1] Department of Climate and Space Sciences and Engineering, University of Michigan, Ann Arbor, Michigan, United States.

[2] Solar System Exploration Division, NASA Goddard Space Flight Center, Greenbelt, Maryland, USA.

[3] Center for Research and Exploration in Space Sciences and Technology II, Catholic University of America, Washington, D.C, USA.

[4] Space Sciences Laboratory, University of California, Berkeley, Berkeley, CA, USA.

[5] Laboratory for Atmospheric and Space Physics, University of Colorado, Boulder, CO, USA.

Key Points:

- Flux ropes form at Mars via three distinct processes: boundary wave instabilities, external reconnection, and internal reconnection.

- Across 1900 orbits, we identify and analyze 121 magnetic flux ropes within the ionosphere of Mars using observations from MAVEN.

- Using electron and magnetic field observations, we separate the flux ropes into three categories based on formation mechanism.

Abstract

Flux ropes are a magnetic field phenomenon characterized by a filament of twisted magnetic field with an axial core and outer helical wraps. They form in the Martian ionosphere via three distinct mechanisms: boundary wave instabilities (BWI), external reconnection (ER) between the interplanetary magnetic field and the crustal anomalies, and internal reconnection (IR) of the crustal anomalies themselves. We have identified 121 magnetic flux ropes from 1900 orbits using plasma and magnetic field measurements measured by the Mars Atmosphere and Volatile EvolutioN (MAVEN) spacecraft, and separate flux ropes into categories based on formation mechanism by analyzing electron signatures. We find evidence for flux ropes formed via BWI, ER, and IR mechanisms which comprise 9%, 34%, and 57% of our dataset, respectively. Flux ropes formed via different mechanisms exhibit differences in location and force-free radius, indicating the formation mechanism of a flux rope impacts their influence on the Martian plasma environment.

Plain Language Summary

Mars possess localized magnetic fields that are frozen into the crust of the planet and protrude out into space. On the dayside of Mars, the crustal fields interact with the charged particles and magnetic field lines that are emanating away from the Sun known as the solar wind. The processes involved in this interaction create the Martian "magnetosphere," and can have a variety of implications on the evolution of the Martian atmosphere. One biproduct of this interaction is a "magnetic flux rope," which is a twisted filament of magnetic flux and plasma. Flux ropes show evidence for the reconfiguration of magnetic field lines within the magnetosphere, and lead to atmospheric loss at Mars. Using data from the Mars Atmosphere and Volatile EvolutioN (MAVEN) spacecraft, we analyze 121 events in which the spacecraft encountered a flux rope along its orbit around Mars. This is the first study to show evidence for Martian flux ropes having been formed via three distinct formation mechanisms. Flux ropes formed via different mechanisms exhibit differences in geographic location and size, indicating the formation mechanism of a flux rope impacts their influence on the Martian magnetospheric and atmospheric environment.

1 Introduction

Magnetic flux ropes are a well-documented space plasma physics phenomenon that have been detected throughout the solar system, ranging from the lower solar corona (*Fillipov et al., 2015*)

52   to the magnetosphere of Saturn (*Jasinski et al., 2016*). An understanding of flux ropes and their

53   formation mechanisms is important for research in all space plasma environments for two main

54   reasons: 1) flux rope formation plays a fundamental role in the reconfiguration of magnetic

55   topology and 2) flux ropes have physical effects on the ambient environment, which includes

56   storing magnetic energy and acting as channels for charged-particle transport. The ubiquity of

57   flux ropes throughout diverse plasma environments suggests various processes are responsible

58   for their formation.

59   At intrinsic magnetospheres, such as Earth and Mercury, planetary flux ropes are frequently

60   observed along the dayside magnetopause and believed to form via multiple X-line reconnection

61   between the interplanetary magnetic field (IMF) and the global intrinsic planetary magnetic field

62   (e.g., *Lee and Fu,* 1985, *Sun et al.,* 2016). Multiple X-line reconnection also occurs to form flux

63   ropes in the cross-tail current sheet where magnetic fields are oppositely oriented in the two

64   lobes (e.g., *Elphic et al.,* 1986, *Slavin et al.,* 2003, *DiBraccio et al.,* 2015). On the dayside of

65   planets with intrinsic magnetic fields, a high shear between the dipole magnetic field and the

66   IMF along the magnetopause may result in single X-line reconnection or multiple X-line

67   reconnection, the latter forming at least two magnetic flux ropes. After their formation on the

68   dayside of the planet, these flux ropes subsequently carry magnetic flux and plasma to the

69   nightside of the planet.

70   Flux ropes have also been observed at Venus, Mars, and Titan where intrinsic planetary magnetic

71   fields are absent (e.g., *Wolff et al.,* 1980, *Luhmann et al.,* 1985, *Cloutier et al.*, 1999, *Penz et al.,*

72   2004*, Martin et al.,* 2020). These flux ropes must form through different processes than those

73   observed at magnetized planets with a global intrinsic magnetic field. For example, the IMF flux

74   tubes penetrate into Venus' ionosphere and drape around the planet. The barrier between the fast

75   moving tailward flows of the magnetosheath and the slower moving ionospheric plasma (i.e., the

76   ionopause) is subject to the development of large amplitude boundary wave instabilities.

77   Simulation results have suggested that boundary wave instabilities such as Kelvin-Helmholtz

78   (KH) may become non-linear and lead to flux rope formation at the ionopause of Venus (e.g.,

79   *Terada et al.,* 2002, *Möstl et al.,* 2011). These flux ropes were observed to be small-scale

80   structures (~10 km in radius) and are evidence for the twisting of draped IMF flux tubes in the

81   ionosphere of Venus (*Luhmann et al.,* 1985).

82 Flux ropes in the Martian induced magnetosphere are of particular interest due to the localized

83 magnetic anomalies preserved by the crust of the planet (*Acuña., et al.,* 1999). In the southern

84 hemisphere, the crustal anomalies are strong (~100-1000 nT at the surface) and protrude into

85 space creating "mini-magnetospheres" similar to the IMF-planetary interactions along the

86 dayside magnetopause of magnetized planets. In the northern hemisphere, the crustal anomalies

87 are much weaker, and do not inhibit the IMF flux tubes from penetrating deep into the

88 ionosphere, creating a plasma environment similar to that at Venus. Together, these two

89 hemispheres comprise a unique hybrid magnetosphere at Mars. Flux ropes play two major roles

90 at Mars: 1) the rapid reconfiguration of planetary crustal magnetic fields and the acceleration of

91 charged particles, and 2) atmospheric mass loss as planetary particles travel through their helical

92 wraps and escape down the magnetotail.

93 Magnetic flux ropes have been observed in the ionosphere of Mars by the Mars Global Surveyor

94 (MGS) (e.g., *Cloutier et al.*, 1999; *Vignes et al.*, 2004; *Briggs et al.*, 2011; *Hara et al.,* 2014) and

95 the Mars Atmosphere and Volatile EvolutioN (MAVEN) spacecrafts (e.g., *Hara et al.,* 2017).

96 The hybrid nature of Mars' magnetosphere suggests that these flux ropes may be created in

97 processes similar to Venusian ionospheric flux ropes formed by KH instabilities, or perhaps by a

98 process unique to the Martian plasma environment. *Brain et al.,* [2010] first reported the MGS

99 observation of a flux rope forming as a result of crustal field detachment due to magnetic

100 reconnection. Using the plasma analysis capabilities of MAVEN, *Hara et al.,* [2017] also

101 provided a detailed analysis of a similar event and demonstrated that this single ionospheric flux

102 rope contained multiple planetary ions including H+, O+, O2+, and likely CO2+.

103 There is evidence that flux ropes at Mars may form via at least of the following three distinct

104 mechanisms:

105   1.The development of large-amplitude boundary wave instabilities (BWI), most probably

106   KH, on the boundary between the fast tailward flows in the magnetosheath and the

107   slowly moving ionospheric plasma, similar to those found on Venus. KH waves have

108   been detected at Mars (*Ruhunusiri et al.,* 2016), and if these boundary waves steepen

109   sufficiently, the IMF flux tubes frozen into the magnetosheath plasma may undergo

110   magnetic reconnection and lead to flux rope formation as illustrated in Figure **1a**.

111   2.Multiple X-line external reconnection (ER) between the draped IMF and a crustal

112   anomaly can form flux ropes in a manner similar to flux rope formation on the dayside

113   magnetopause of intrinsically magnetized planets (*Hara et al.,* 2014, *Hara et al.,* 2017),

114   illustrated in Figure **1b**.

115   3. Single X-line internal reconnection (IR) of the crustal anomalies themselves (e.g., *Brain*

116   *et al.,* 2010, *Beharrell et al.,* 2012, *Hara et al.,* 2014). As the solar wind plasma flows

117   around Mars, the ram pressure may distort the crustal anomalies as they respond to

118   maintain pressure balance, leading to single X-line reconnection between the field lines

119   of the anomalies themselves resulting in flux rope formation illustrated in Figure **1c**.
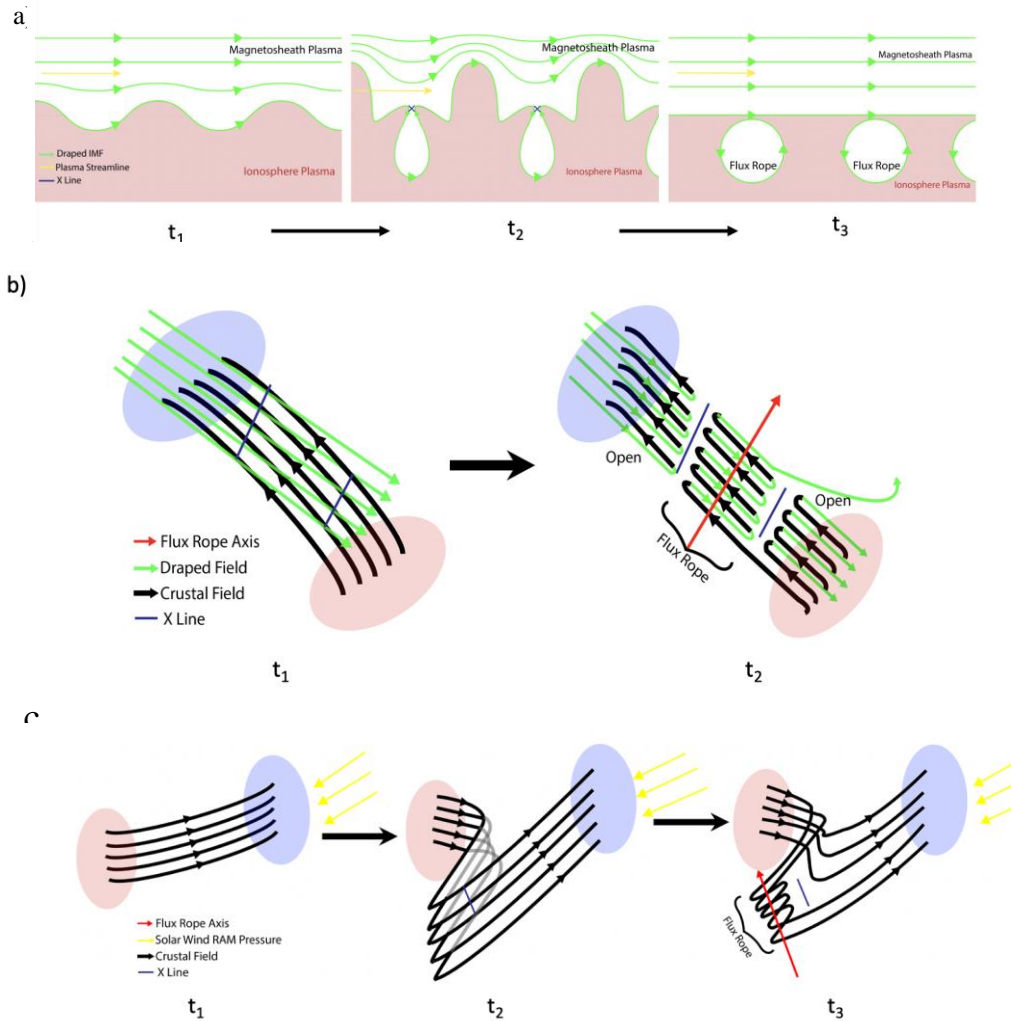
Figure **1**: *(a) Schematic demonstrating how a flux rope may form under the boundary wave instability mechanism, (b) external reconnection mechanism, and (c) internal reconnection mechanism. Red and blue ovals represent regions of crustal fields that point radially outward and inward, respectively. Black arrows represent crustal magnetic field lines, green arrows represent draped IMF field lines, yellow arrows represent flowing sheath plasma streamlines, blue lines or X's represent X-lines.*

120 Observations of flux ropes in the Martian ionosphere provide direct evidence for boundary wave

121 instabilities or crustal field magnetic reconnection; however, there has been no comprehensive

122 study of ionospheric flux ropes using the measurement capabilities of MAVEN to investigate

123 their formation mechanisms. The work presented here conducts an extensive survey of flux ropes

124 in the ionosphere of Mars. We use plasma data measured by MAVEN to estimate the magnetic

125 topology of the flux ropes, providing evidence for three distinct formation mechanisms at Mars.

126 Further analysis of the plasma contained within the flux ropes contributes to the fascinating topic

127 of atmospheric mass loss at Mars.

128 **2 Materials and Methods**

129 2.1 Instrumentation

130 We investigate Martian flux ropes and their impact on the global magnetosphere and ionosphere

131 through an analysis of data provided by the MAVEN spacecraft (*Jakosky et al.,* 2015).

132 MAVEN's orbit precesses in both local time and longitude to provide global coverage of the

133 Mars atmosphere and space environment with periapsis at ~150 km and apoapsis reaching ~6200

134 km. In particular, we analyze data provided by the Magnetometer (MAG) instrument (*Connerney*

135 *et al.,* 2015) which measures vector magnetic fields at a maximum sampling rate of 32 vectors/s,

136 the Solar Wind Electron Analyzer (SWEA) (*Mitchell et al.,* 2016), and the SupraThermal And

137 Thermal Ion Composition (STATIC) instrument (*McFadden et al.*, 2015).

138 2.2 Methodology

139 Here, MAG data are analyzed in the Mars Solar Orbiter (MSO) and Minimum Variance Analysis

140 (MVA) coordinate system. The MSO coordinate system is defined so that the X-axis points from

141 the center of Mars towards the Sun, the Z-axis points towards geographic north, and the Y-axis

142 completes the right-handed coordinate system. Magnetic flux rope signatures identified in the

143 MAG data depend heavily on the orientation of the flux rope, as well as the spacecraft trajectory

144 through the flux rope structure. In order to account for this variability, we transform the magnetic

145 field data into MVA coordinates (*Sonnerup and Scheible,* 1998). In the MVA coordinate system

146 for a flux rope, the N-direction defines the axis along which the magnetic field varies the least

147 (i.e., minimum variance axis), and the N component (B_N) of the magnetic field remains steady

148 throughout the extent of a flux rope. Note, the mean value of the B_N component of the magnetic

149   field is smallest for spacecraft trajectories that pass closest to the center of quasi-cylindrical flux

150   ropes. The M-direction (intermediate variance) points orthogonal to the N-direction and along

151   the central axis of quasi-force free flux ropes (*Slavin et al.,* 2003). B_M for a flux rope would

152   therefore exhibit a unimodal peak corresponding to the axial field enhancement at the center of

153   the flux rope. The L-direction (maximum variance) completes the right-handed coordinate

154   system and points in the direction of the bipolar magnetic field (B_L) signature defined by the

155   outer helical wraps. The full amplitude of this bi-polar B_L flux rope signature maximizes for

156   spacecraft trajectories passing closest to the central axis of the flux rope.

157   We also analyze superthermal ($>$1eV) electron data from the SWEA instrument onboard

158   MAVEN to estimate the source of the electrons that populate the flux rope and the surrounding

159   plasma environment, as well as the magnetic topology. SWEA is capable of measuring electron

160   fluxes at a 4 second cadence. We use these fluxes compared to the local magnetic field

161   orientation and spacecraft location to parameterize the electron distribution as demonstrated by

162   *Weber et al.,* 2017. This parameter is known as the pitch angle distribution (PAD) score and is

163   defined by: (fFA- fperp)/σ , where fFA is the electron flux in the field aligned direction (the most

164   field-aligned 10° available within pitch angles s 0-30° and 150-180°), fperp is the electron flux in

165   perpendicular direction (pitch angles 85-95°), and σ is the propagated uncertainty. PAD score

166   distinguishes among 3 electron distributions: (1) field-aligned beam distribution (PAD score $>$2),

167   (2) isotropic distribution (- 3$<$ PAD score $<$2), (3) loss cone distribution (PAD score $<$-3). We

168   also compare the electron energy distribution to an expected distribution for photoelectrons at

169   Mars to parameterize the likelihood that the measured electrons are composed of primarily

170   photoelectrons or solar wind electrons (*Xu et al.,* 2017); this is known as the shape parameter.

171   The shape parameter distinguishes between two electron populations: 1) photoelectrons (shape

172   parameter $<$ 1) and 2) solar wind electrons (shape parameter $>$ 1). Both the PAD score and shape

173   parameter are calculated for populations that are moving towards Mars and away from Mars by

174   measuring the local inclination of the magnetic field and comparing it with the pitch angle

175   distribution of the electrons. We compare all these parameters measured at a single time step to

176   arrive at an estimation for the magnetic topology at the spacecraft's location (*Xu et al.,* 2019).

177   The topology score can distinguish among 7 different topologies, which are numbered 1-7, with

178   0 indicating the data were insufficient to determine the topology.

179   MAVEN has a precessing elliptical orbit where the spacecraft samples throughout the

180   magnetosphere and into the solar wind. This ensures that there are extended periods in which the

181   spacecraft does not sample near dayside of Mars, where we assume most of the ionospheric flux

182   ropes are formed. Therefore, we selected for orbits that sampled the low altitude (<1200 km)

183   near-dayside (solar zenith angle (SZA) <110°) of the planet and visually inspected the MAG data

184   for flux rope signatures.

3 Results

186   Throughout the 1900 orbits inspected, we identified 171 magnetic flux ropes. Of the 171 flux

187   ropes identified, 156 show a sufficiently large (>2) max/intermediate eigenvalue ratio calculated

188   from MVA. In MVA, the max/intermediate eigenvalue ratio is an indication of the accuracy of

189   the coordinate definition. These flux ropes display a wide range in core field intensity (5-110

190   nT), and location in latitude (-75° - +75°) and longitude (1° - 358°). Of the 156 flux ropes

191   selected, 140 contain sufficient electron data from SWEA to estimate magnetic topology. Below

192   160 km altitude, the superthermal electrons are dominated by local processes such as production

193   and collisions which makes the topology score unreliable (*Xu et al.,* 2019). We therefore omit

194   flux rope events that were detected below 160 km, leaving us with 121 events. The flux ropes

195   that comprise our database exhibit three primary magnetic topologies (draped, open-dayside,

196   closed-dayside). This variety in magnetic topology suggests that these flux ropes may have been

197   formed via different formation mechanisms.

198   In order to categorize the formation mechanism of each flux rope, we examine the MAG,

199   SWEA, and STATIC data that are available for each event. Depending on the signatures, a flux

200   rope is assigned a formation mechanism of BWI, ER, or IR based on the following observations:

201   if a flux rope were to form via the BWI mechanism, it would be populated primarily by electrons

202   that have been traveling with the flow of the solar wind and the magnetic field lines would be

203   connected on both ends to the IMF, which is classified as a draped magnetic field line. Thus, a

204   draped topology score throughout a flux rope suggests that it had been formed via the BWI

205   mechanism. If a flux rope were formed via the ER mechanism, the "opening up" of crustal

206   magnetic field lines would allow solar wind plasma to mix with the ionospheric plasma that

207   previously populated the closed magnetic loops of the crustal anomalies. Thus, flux ropes formed

208   via the ER mechanism would contain both solar wind electrons and photoelectrons and exhibit

209   open-dayside magnetic field topology. If a flux rope were to form via the IR mechanism, the flux

210   rope would be surrounded by closed magnetic topology and contain exclusively photoelectrons

211   because the flux rope does not require any reconnection involving the IMF. Thus, flux ropes that

212   exhibit closed-dayside magnetic topology throughout their structure are consistent with having

213   been formed via the IR mechanism.

214   3.1 Case Studies

215   Figure **2** shows a time series of a flux rope signature in the MAVEN data. The flux rope can be

216   identified by a characteristic increase in total magnetic field amplitude (Figure **2b**), and a

217   unimodal peak in B_M coinciding with the inflection point of a bipolar signature in B_L (Figure **2c**).

218   The shape parameter is >1 in both the away and towards directions throughout the flux rope

219   signature (Figure **2e**), indicating that the flux rope is populated primarily by solar wind electrons
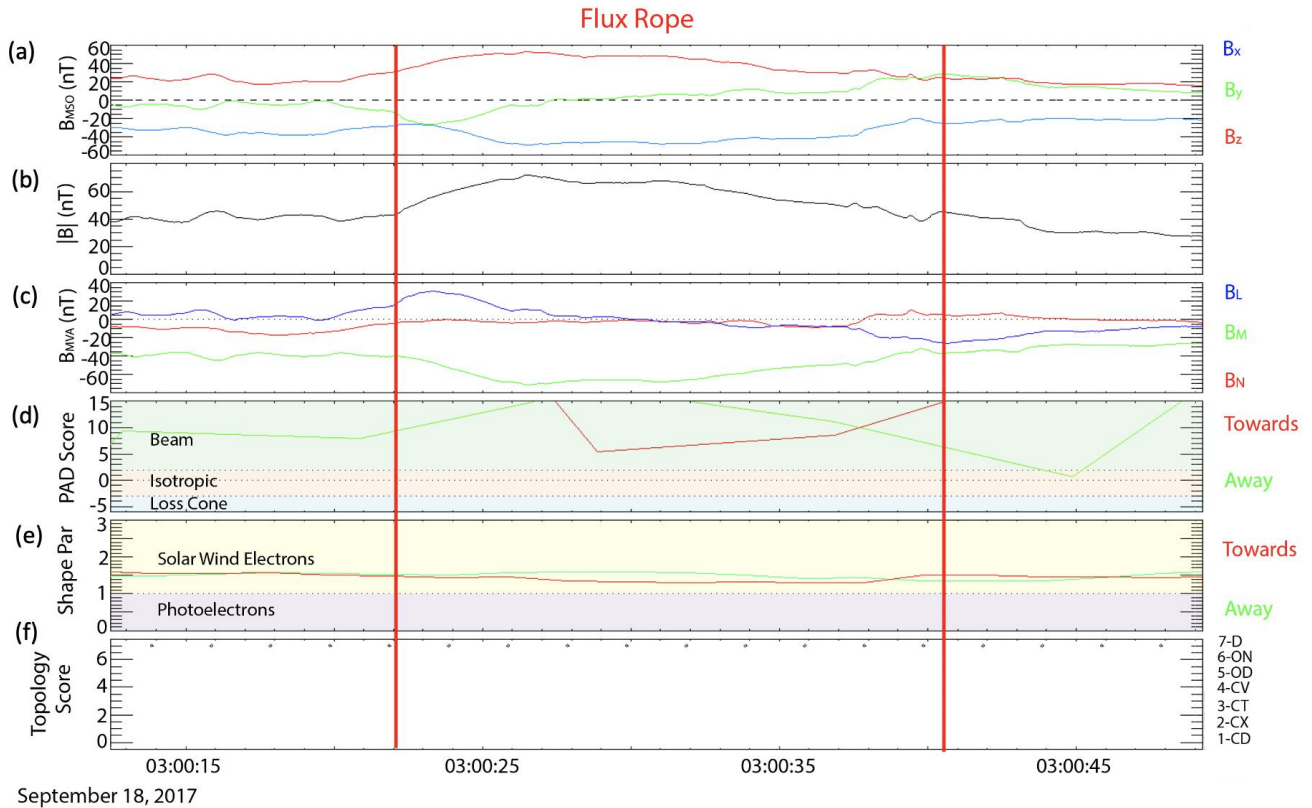

Figure **2**: *MAVEN observations of a flux rope detected on September 18, 2017, a) magnetic field in the MSO frame, b) magnetic field magnitude, c) magnetic field in MVA coordinate frame, d) PAD score, e) shape parameter, f) topology score*

220   rather than photoelectrons in both the away and towards direction. Therefore, the topology score

221   throughout the flux rope is 7 (Figure **2f**), which indicates draped magnetic topology. Draped

222   magnetic topology is expected if the flux rope were to have been formed via the BWI mechanism

223   illustrated in Figure **1a**. Of the 121 flux ropes in our database, 11 (9%) are consistent with

224   hsaving been formed via the BWI formation mechanism.

225   Figure **3** shows a time series of a pair of flux ropes detected by MAVEN on May 14, 2018. From

226   the onset of the first flux rope to ~18:52:30 the shape parameter is < 1 (Figure **3e**) and the

227   topology score is = 1 (Figure **3f**), indicating the presence of photoelectrons and closed-dayside

228   magnetic topology. For the remainder of the flux rope, the shape parameter in the towards

229   direction remains >1, and the topology score is = 5, indicating the presence of solar wind

230   electrons and open-dayside magnetic topology. Open-dayside magnetic topology is expected if

231   the flux rope were to have been formed via the ER mechanism illustrated in Figure **1b**. 41 (34%)

232   of flux ropes in our database are consistent with having been formed via the ER formation
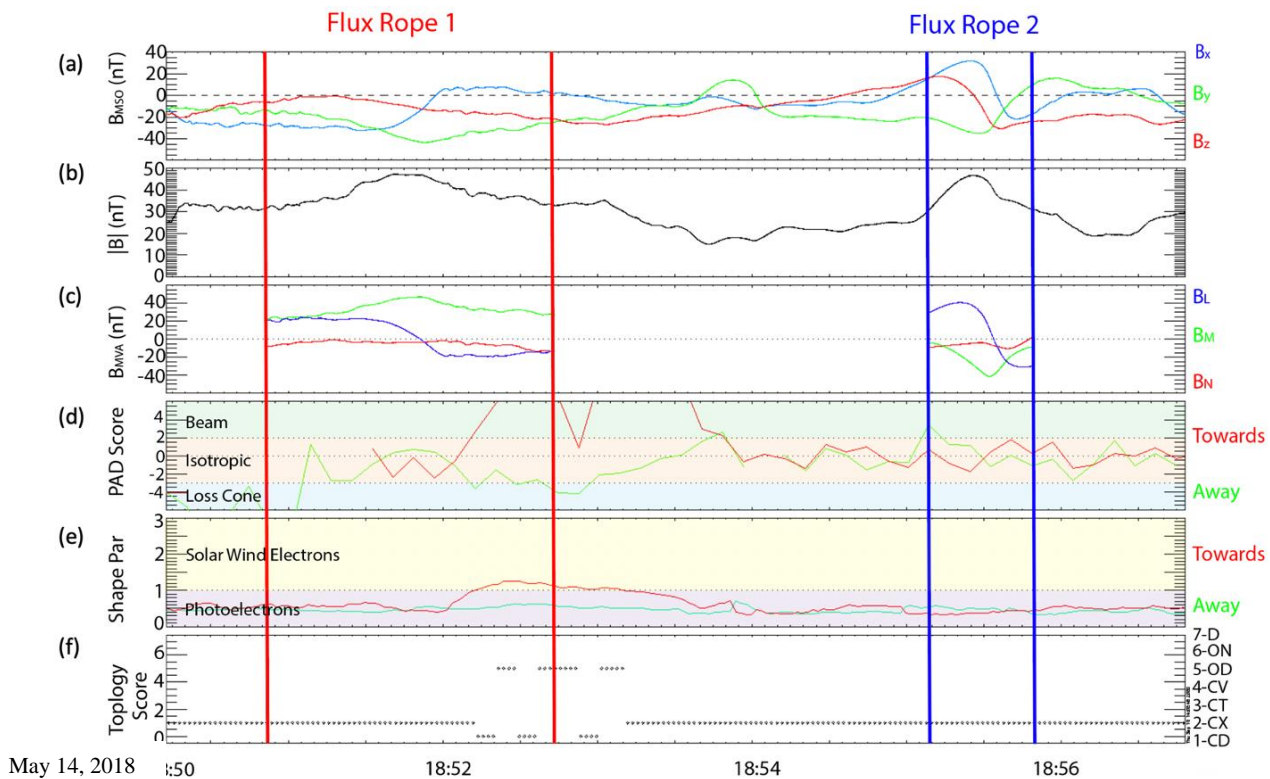
233   mechanism.

Figure **3**: MAVEN observations on May 14, 2018 in the same format as Figure **1**.

234   The second flux rope shown in Figure **3** maintains a shape parameter <1 and a topology score of

235   1 throughout the structure, indicating the presence of photoelectrons and closed-dayside

236   magnetic topology, respectively. Closed-dayside topology is expected if the flux rope were to

237   have been formed via the IR mechanism illustrated in Figure **1c**. 69 (57%) of the flux ropes in

238   our database are consistent with having been formed via the IR formation mechanism.

4 Discussion

240   Figure **4a** shows a histogram of altitudes at which flux ropes were detected, separated by

241   formation mechanism. BWI flux ropes tend to occur at higher altitudes (median altitude = 670

242   km) than ER or IR flux ropes (median altitudes = 222 and 198 km, respectfully), which is

243   consistent with the idea that BWI flux ropes form closer to the boundary between the

244   magnetosheath and ionospheric plasma. Furthermore, Figure **4b** shows the occurrence rate of

245   flux ropes measured by MAVEN in different latitude bins. BWI flux ropes tend to occur more

246   frequently near the poles. This is consistent with BWI flux ropes forming as a result of velocity
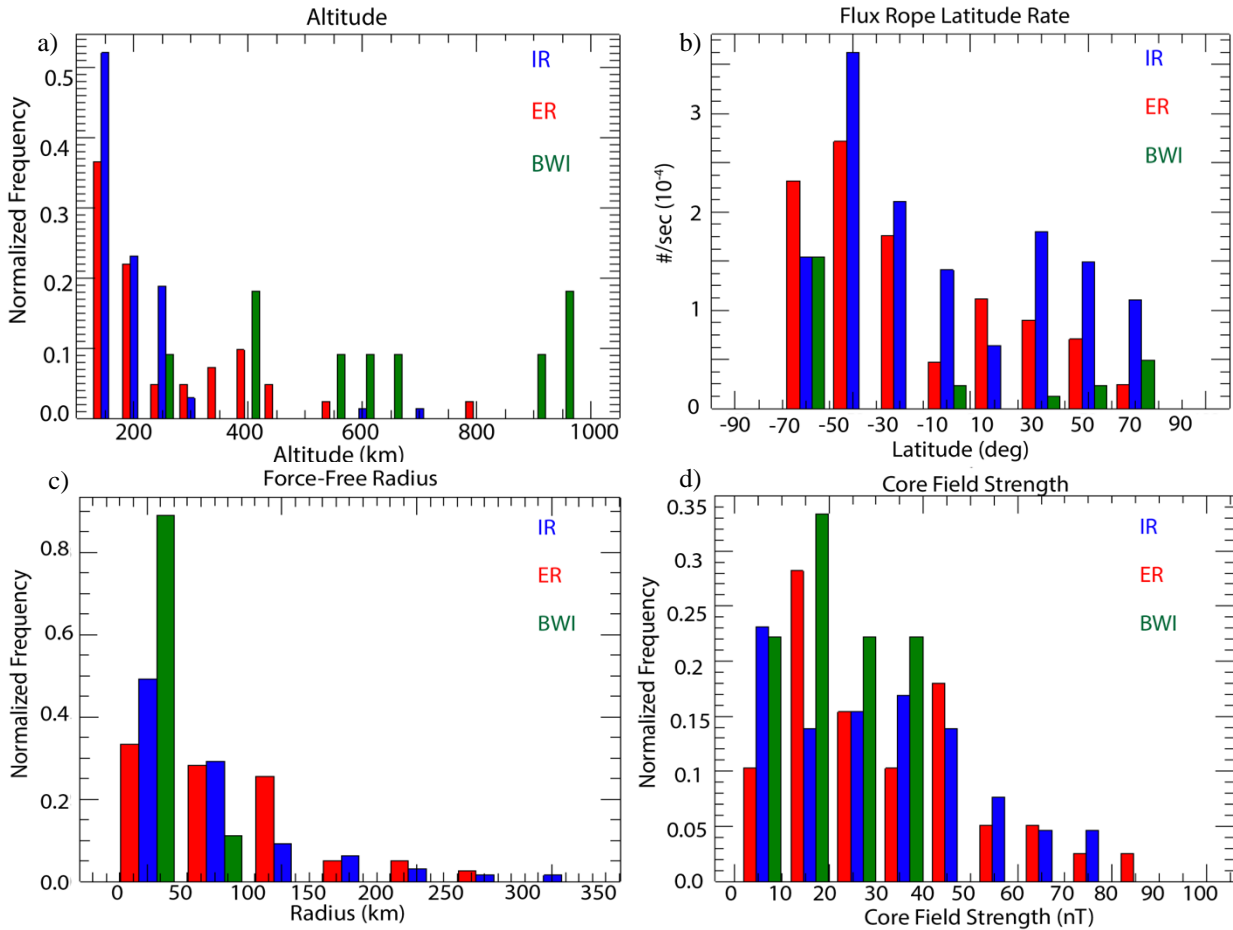

Figure **4**: *Flux rope properties separated by formation mechanism: a), Altitude at which the flux ropes were detected (km), b) flux rope occurrence rate at different latitudes (flux ropes/ second), c) flux rope radius estimated by the force-free model fit (km), d) Maximum field strength of the core field estimated by the force-free model (nT)*

247   shear because we expect the gradient between magnetosheath and ionospheric plasma to be

248   greatest near the terminators. The ER and IR flux ropes occur most frequently in the mid-

249   southern latitudes where the crustal magnetic fields are strongest, which is consistent with the

250   notion that they were formed via reconnection between an anomaly and the IMF (ER), or

251   reconnection of the crustal anomalies themselves (IR).

252   We implement a model in which flux ropes are assumed to be force-free ($\vec{J} \times \vec{B} = 0$) and

253   stationary in order to estimate other properties of the flux ropes including radii and core-field

254   strength at the center of the structure. Assuming cylindrical symmetry, *Lepping et al.,* 1996

255   showed that the axial and tangential magnetic field of a flux rope can be expressed with Bessel

256   functions:

$$B_A = J_0(\alpha r')B_0, \qquad B_T = J_1(\alpha r')B_0 H, \qquad B_r = 0$$

257   B_A, B_T, B_R are the axial, tangential, and radial magnetic fields, $J_0(\alpha r')$, $J_1(\alpha r')$ are the zeroth-

258   and first-order Bessel functions, B_0 is the magnetic field magnitude of the flux rope's core, and

259   H is the handedness of the helicity. The parameter α is a constant at 2.4048 and represents the x-

260   intercept of the zeroth-order Bessel function. The components of this modeled field thus depend

261   on r', which is the radial distance from the center of the flux rope. We can apply this fitting

262   technique to all 113 events in this study and implement a χ^2 test to select a radius that produces a

263   best fit for each flux rope event. This best fit radius also allows us to estimate the absolute core-

264   field strength of each event. Selecting for events where $\chi^2 < .02$, we find that 102 of the 121

265   flux ropes can be considered force-free. Of these 102 flux ropes, we see a great variety of radius

266   estimates (2 km – 311 km) and core-field strength (6-110 nT). There is a strong linear correlation

267   between impact parameter of the flux rope crossing determined by the force-free fitting and the

268   normalized mean value of the N component of the magnetic field ($|B_N|/B_{max}$), where B_{max} is the

269   maximum field strength within the flux rope (not shown). This correlation suggests that the

270   MVA and force-free fitting analysis are in agreement.

271   We produce a histogram of radius and core-field strength separated by estimated flux rope

272   formation mechanism (Figure **4c**, **4d**). Flux ropes formed through ER, IR have median radii of

273   64, 50 km, respectively. Flux ropes formed through BWI are the smallest of the three

274   mechanisms, with a median radius of 5 km. This radius is in agreement with flux ropes found at

275   Venus which have an estimated radius of ~10 km (*Luhmann et al.,*1985), further suggesting that

276   these flux ropes may have formed via a process similar to that at unmagnetized objects like

277   Venus and Titan. Using data from the STATIC instrument, we are able to estimate the local

278   gyroradius for three main species in the Martian ionosphere: H^+, O^+, and O_2^+ (median local

279   gyroradii of 11 km, 74 km, and 113 km, respectively). If the radius of a flux rope is smaller than

280   the gyroradius of a particle, then the particle cannot be frozen into the magnetic field of the flux

281   rope, and the flux rope could not be a mechanism for ionospheric escape at Mars. Of the 102 flux

282   ropes that are considered force-free, 77 (75%), 50(47%), and 41 (40%) have radii larger than the

283   local gyroradius of H^+, O^+, and O_2^+ , respectively. This suggests that only a fraction of the flux

284   ropes found in our database may contribute to the escape of planetary ions. While the efficiency

285   of flux ropes ability to trap ionospheric H^+ does not depend on formation mechanism, no BWI

286   flux ropes are large enough to trap O^+ or O_2^+ ions, suggesting BWI flux ropes are not an efficient

287   mechanism for planetary ion escape. There is no significant difference between the IR and ER

288   flux ropes in their ability to lead to ionospheric escape via plasma entrainment and propagation

289   downstream. The core-field strength of the BWI, ER, and IR flux ropes does not vary greatly

290   depending on formation mechanism (median values of 25 nT, 33 nT, 33 nT, respectively).

291   This is the first study that examines these three flux rope formation mechanisms using

292   observations and statistics. The magnetosphere of Mars offers scientists a unique opportunity to

293   study flux rope formation processes at a single object. This allows for fascinating comparisons

294   among the properties of, and conditions that favor, flux rope formation at the planet. Our future

295   work will investigate the dependency of flux rope formation on upstream solar wind conditions

296   to better our understanding of the complex interaction between the solar wind and Martian

297   plasma environments.

298   **5 Summary**

299   We visually inspected over 1900 orbits in which MAVEN sampled the dayside ionosphere of

300   Mars. We transformed the MAG data into MVA coordinates to identify 156 magnetic flux ropes

301   within the Martian ionosphere. Electron data from the SWEA instrument was used to determine

302   magnetic topology of the flux ropes in order to estimate their formation mechanism. Each of the

303   three magnetic topologies (draped, open-dayside, closed-dayside) that comprise the flux ropes

304   within our database are consistent with a distinct formation mechanism: 1) boundary wave

305   instabilities (BWI) like KH similar to flux ropes observed at Venus 2) external reconnection

306   (ER) between the IMF and the crustal anomalies 3) internal reconnection (IR) of the crustal

307 anomalies themselves. The BWI flux ropes are the least common in our dataset, making up only

308 9% of the flux ropes, while the ER and the IR formation mechanisms make up 33% and 58% of

309 the flux ropes, respectively. Using a force-free model fit, we were able to estimate the radii and

310 core-field strength of the 129 flux ropes. The radii of flux ropes range from 2 km-360 km, and

311 the core-field strength range from 5 nT-110 nT. Interestingly, the properties of BWI flux ropes

312 including altitude at which they are detected, latitude, and median radius differ from the ER and

313 IR flux ropes. Comparisons between the local gyroradii of planetary ions and the radii of the flux

314 ropes suggests that roughly a third of the ER and IR flux ropes are large enough to trap heavy

315 ions like O^+ and O_2^+, while no BWI flux ropes are sufficiently large to trap heavy ions.

316 **Acknowledgments, Samples, and Data**

320

321 **References**

322 Acuña, M. H., et al. (1999), Global distribution of crustal magnetization discovered by the mars

323 global surveyor MAG/ER experiment, Science, 284(5415), 790-793.

324

325 Beharrell, M., and J. Wild (2012), Stationary flux ropes at the southern terminator of Mars,

326 Journal of Geophysical Research-Space Physics, 117(A12).

327

328 Brain, D., A. Baker, J. Briggs, J. Eastwood, J. Halekas, and T. Phan (2010), Episodic detachment

329 of Martian crustal magnetic fields leading to bulk atmospheric plasma escape, Geophysical

330 Research Letters, 37.

331

332 Briggs, J., D. Brain, M. Cartwright, J. Eastwood, and J. Halekas (2011), A statistical study of

333 flux ropes in the Martian magnetosphere, Planetary and Space Science, 59(13), 1498-1505.

334 Cloutier, P., et al. (1999), Venus-like interaction of the solar wind with Mars, Geophysical

335 Research Letters, 26(17), 2685-2688.

336

337 Connerney, J., J. Espley, P. Lawton, S. Murphy, J. Odom, R. Oliversen, and D. Sheppard (2015),

338 The MAVEN Magnetic Field Investigation, Space Science Reviews, 195(1-4), 257-291.

339 DiBraccio, G., et al. (2015), MESSENGER observations of flux ropes in Mercury's magnetotail,

340 Planetary and Space Science, 115, 77-89.

341

342 Elphic, R., C. Cattell, K. Takahashi, S. Bame, and C. Russell (1986), ISEE-1 and ISEE-2

343 Observations of Magnetic-Flux Ropes in the Magnetotail - FTES in the Plasma Sheet,

344 Geophysical Research Letters, 13(7), 648-651.

345

346 Filippov, B., O. Martsenyuk, A. Srivastava, and W. Uddin (2015), Solar Magnetic Flux Ropes,

347 Journal of Astrophysics and Astronomy, 36(1), 157-184.

348

349 Fu, Z., and L. Lee (1985), Simulation of Multiple X-Line Reconnection at the Dayside

350 Magnetopause, Geophysical Research Letters, 12(5), 291-294.

351

352 Hara, T., K. Seki, H. Hasegawa, D. Brain, K. Matsunaga, M. Saito, and D. Shiota (2014),

353 Formation processes of flux ropes downstream from Martian crustal magnetic fields inferred

354 from Grad-Shafranov reconstruction, Journal of Geophysical Research-Space Physics, 119(9),

355 7947–7962.

356

357 Hara, T., et al. (2017), MAVEN observations of a giant ionospheric flux rope near Mars resulting

358 from interaction between the crustal and interplanetary draped magnetic fields, Journal of

359 Geophysical Research-Space Physics, 122(1), 828-842.

360

361 Jakosky, B. M., M. Slipski, M. Benna, P. Mahaffy, M. Elrod, R. Yelle, S. Stone, and N. Alsaeed

362 (2017), Mars' atmospheric history derived from upper-atmosphere measurements of, Science,

363 355(6332), 1408-1410.

364 Jasinski, J., J. Slavin, C. Arridge, G. Poh, X. Jia, N. Sergis, A. Coates, G. Jones, and J. Waite

365 (2016), Flux transfer event observation at Saturn's dayside magnetopause by the Cassini

366 spacecraft, Geophysical Research Letters, 43(13), 6713-6723.

367

368   Lepping, R., J. Slavin, M. Hesse, J. Jones, and A. Szabo (1996), Analysis of magnetotail flux
369   ropes with strong core fields: ISEE 3 observations, Journal of Geomagnetism and Geoelectricity,
370   48(5-6), 589-601.

371

372   Luhmann, J., and R. Elphic (1985), On the Dynamo Generation of Flux Ropes in the Venus
373   Ionosphere, Journal of Geophysical Research-Space Physics, 90(NA12), 2047-2056.

374

375   Martin, C., C. Arridge, S. Badman, C. Russell, and H. Wei (2020), Distribution and Properties of
376   Magnetic Flux Ropes in Titan's Ionosphere, Journal of Geophysical Research-Space Physics,
377   125(4), 1029-1043.

378

379   McFadden, J., et al. (2015), MAVEN SupraThermal and Thermal Ion Compostion (STATIC)
380   Instrument, Space Science Reviews, 195(1-4), 199-256.

381

382   Mitchell, D., et al. (2016), The MAVEN Solar Wind Electron Analyzer, Space Science Reviews,
383   200(1-4), 495-528.

384

385   Möstl, U., N. Erkaev, M. Zellinger, H. Lammer, H. Groller, H. Biernat, and D. Korovinskiy
386   (2011), The Kelvin-Helmholtz instability at Venus: What is the unstable boundary?, Icarus,
387   216(2), 476-484.

388

389   Penz, T., et al. (2004), Ion loss on Mars caused by the Kelvin-Helmholtz instability, Planetary
390   and Space Science, 52(13), 1157-1167.

391

392   Ruhunusiri, S., et al. (2016), MAVEN observations of partially developed Kelvin-Helmholtz
393   vortices at Mars, Geophysical Research Letters, 43(10), 4763-4773.

394

395   Slavin, J., R. Lepping, J. Gjerloev, D. Fairfield, M. Hesse, C. Owen, M. Moldwin, T. Nagai, A.
396   Ieda, and T. Mukai (2003), Geotail observations of magnetic flux ropes in the plasma sheet,
397   Journal of Geophysical Research-Space Physics, 108(A1), 1015-1033.

398

399   Sonnerup, B. U. Ö., and M. Scheible (1998), Minimum and maximum variance analysis, in

400   Analysis Methods for Multi-Spacecraft Data, ISSI Sci. Rep. no. SR-001, edited by G.

401   Paschmann and P. W. Daly, chap. 8, pp. 185–220, European Space Agency, Noordwijk,

402   Netherlands.

403

404   Sun, W., S. Fu, J. Slavin, J. Raines, Q. Zong, G. Poh, and T. Zurbuchen (2016), Spatial

405   distribution of Mercury's flux ropes and reconnection fronts: MESSENGER observations,

406   Journal of Geophysical Research-Space Physics, 121(8), 7590-7607.

407

408   Terada, N., S. Machida, and H. Shinagawa (2002), Global hybrid simulation of the Kelvin-

409   Helmholtz instability at the Venus ionopause, Journal of Geophysical Research-Space Physics,

410   107(A12), 1471.

411

412   Vignes, D., M. Acuna, J. Connerney, D. Crider, H. Reme, and C. Mazelle (2004), Magnetic flux

413   ropes in the Martian atmosphere: Global characteristics, Space Science Reviews, 111(1-2), 223-

414   231.

415

416   Weber, T., D. Brain, D. Mitchell, S. Xu, J. Connerney, and J. Halekas (2017), Characterization

417   of Low-Altitude Nightside Martian Magnetic Topology Using Electron Pitch Angle

418   Distributions, Journal of Geophysical Research-Space Physics, 122(10), 9777-9789.

419

420   Wolff, R. S., B. E. Goldstein, and C. M. Yeates (1980), The onset and development of Kelvin-

421   Helmholtz instabilities at the Venus ionopause, Journal of Geophysical Research: Space Physics,

422   85(A13), , 7697–7707.

423

424   Xu, S., T. Weber, D. Mitchell, D. Brain, C. Mazelle, G. DiBraccio, and J. Espley (2019), A

425   Technique to Infer Magnetic Topology at Mars and Its Application to the Terminator Region,

426   Journal of Geophysical Research-Space Physics, 124(3), 1823-1842.

427

428   Xu, S., et al. (2017), Martian low-altitude magnetic topology deduced from MAVEN/SWEA

429   observations, Journal of Geophysical Research-Space Physics, 122(2), 1831-1852.

430